Optimization of Lead Design and Electrode Configuration in Deep Brain Stimulation

Ruben Cubo

Department of Information Technology
Uppsala University
Box 337
751 05 Uppsala, Sweden
Email: ruben.cubo@it.uu.se

Mattias Åström

Department of Biomedical Engineering
Linköping University
581 85 Linköping, Sweden
Email: matas@imt.liu.se

Alexander Medvedev

Department of Information Technology
Uppsala University
Box 337
751 05 Uppsala, Sweden
Email: am@it.uu.se

Abstract—Deep Brain Stimulation (DBS) is a medical treatment whose exact underlying biological mechanism is unknown. Yet, DBS is an established therapy in a number of neurological and mental disorders. Mathematical models aiming at a better understanding of DBS through the simulation of the electrical field in the brain have been developed in the past years. This study covers *in silico* optimization of the electrical stimuli delivered to the brain by means of a Finite Element model individualized through medical imaging data. The goal is to cover a given target volume with stimulation for full therapeutic effect while limiting the spread of the stimuli beyond the target border, to avoid undesirable side effects. The fraction of the activated tissue volume within the target and the fraction of the stimulation field that spreads beyond it are computed in order to quantify the performance of the stimuli. Two readily available leads are treated: a state-of-the-art lead using single active contact and a field-steering one in multiple active contact stimulation. Further, in order to obtain insights into lead design, hypothetical leads with different geometric characteristics are as well considered. The obtained results suggest that simplified models give a reasonably good approximation to optimal contact selection when compared to clinical data. Configurations with multiple active contacts might improve stimulation in some cases, although there is no general tendency. The lead design study suggests that row segmentation with three or four contacts per row is a good option. In addition, the stimulation performance was generally better for the designs where the contacts were closer to each other. This study thus confirms the importance of mathematical modeling in DBS as an inexpensive way of obtaining optimal stimulation settings and lead designs.

Keywords–Deep Brain Stimulation; Optimization; Lead Design; Convex optimization; Field Steering; Parkinson Disease.

I. INTRODUCTION

Deep Brain Stimulation (DBS) is a surgical procedure that consists of delivering electrical stimuli, usually rectangular biphasic pulses, to a certain target in the brain by using one or several surgically implanted leads. Initially DBS was considered a purely medical problem. However, nowadays there is a lot of interest in the engineering community, e.g., by suggesting alternative set ups based on modeling [1]. The goal of the therapy is the alleviation of symptoms of various neurological diseases, such as Parkinson's Disease (PD) [2], epilepsy [3], dystonia [4], and others. DBS has mostly replaced surgical lesioning and ablation procedures because of its reversibility, flexibility, and individualization potential [5]. The interest in DBS has spread to other areas of medicine and applied to treatment of psychiatric diseases,

such as e.g., schizophrenia [6] or Tourette Syndrome [7]. In the case of PD, since the implantation and programming procedure is quite complicated and costly compared to pharmacotherapy [8], [9], physicians usually choose advanced patients for this procedure, when drugs such as levodopa have lost effectiveness or have severe side effects [2] such as fluctuations, dyskinesias or toxicity [10]. Some studies suggest in fact that an earlier implantation could be beneficial [11].

The principle of DBS is in delivering mild electrical pulses via a chronically implanted lead, whose active contacts are positioned in the subcortical area, where a stimulation target is usually defined. Prior to the operation, patients undergo an extensive clinical examination as well as medical imaging. Based on the images, the physician pinpoints a target area, which is in PD usually located in the basal ganglia, with the subthalamic nucleus (STN) being of particular interest. A few weeks after the surgery, the patients undergo a lengthy trial-and-error programming period to properly tune the stimuli.

Since the underlying physiological mechanism of DBS and its long-term effects on the brain still remain unknown, the therapeutical outcome is difficult to predict. Furthermore, because of uncertainties in the position of the lead or suboptimal stimulation settings, the stimulated volume might go beyond the target causing undesirable side effects [12]. Shaping the stimuli so that the stimulated volume covers the intended target and does not spill outside of it is thus important for maximization of the therapeutical benefits and minimization of the side effects.

Currently used lead designs (see Fig. 1(a)) were originally adopted from cardiac pacing technology [13] and have not evolved much since then. Meanwhile, further insights into neuromodulation obtained in recent years by using computer modeling based in Finite Element Method (FEM), multiphysics simulation and neuron models, along with the exponential improvement of computational capabilities, open up for more sophisticated and individualized solutions. The aim of these is to shorten the programming time and to better understand the underlying mechanisms [14].

Addressing the shortcomings of the currently used designs, novel DBS electrodes have been developed by such companies as Boston Scientific (USA), St. Jude (USA) and Sapiens (The Netherlands, now part of Medtronic). These leads could be configured in more versatile spacial settings and take advantage of field steering techniques to shape the stimuli. As seen from the geometry of the lead contacts in Fig. 1,
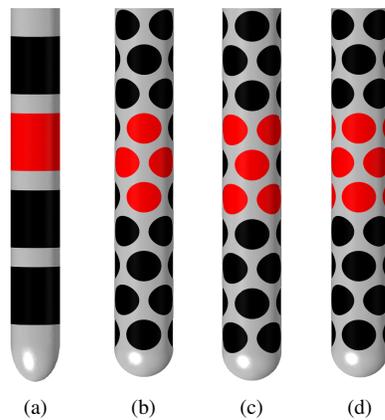
Figure 1. Lead configurations for the conventional lead (a), field-steering Diamond-4 (b), X-5 (c) and X-8 (d). Active contacts are marked in red.

while the conventional state-of-the-art lead delivers a radially symmetric stimulation over the whole cylindrical contact, the field steering one is capable of asymmetrical stimulation that can be tailored to the target area anatomy [15].

Apart from the existing electrodes, hypothetical ones can be tested inexpensively by using realistic computer models. Analysis of design degrees of freedom in novel leads can be performed as well, going beyond the ones already in clinical usage or in development. Segmentation schemes were analyzed in [16] while row separation as a design degree of freedom was treated in [17] and [18]. This study compares the performance of different lead schemes with respect to row segmentation and the separation between the rows, see Fig. 2. At the moment, it is a topic receiving close review, with some of the companies mentioned above already developing schemes with optimized geometry.
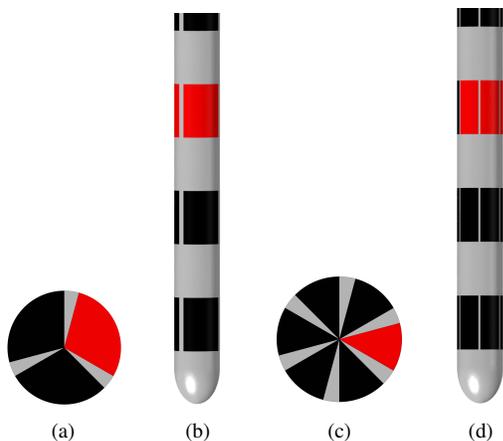

Figure 2. Examples of proposed lead designs: 3 contacts per row (a,b) and 6 contacts per row (c,d). Examples of active contacts are marked in red.

Another possibility for electrode performance improvement is offered by a multicontact stimulation approach, i.e., manipulating the stimuli simultaneously at two or more active contacts. It allows further shaping of the activated tissue volume, thus providing more flexibility.

This study focuses on stimuli optimization using the aforementioned leads, i.e., how to choose a configuration such that a target volume, given by the STN or other volumes, is stimulated. Due to the possible side effects, the stimulation should be kept low outside the target. Within this framework, the objectives of the present study are:

- To compare the optimization results for a state-of-the-art lead to the active contact and to the stimulation amplitude in clinical data, which are assumed to provide good outcome. Both single contact and multicontact approaches are evaluated.

- To optimize a field steering lead over a set of contact configurations and compare to the state-of-the-art lead, in order to assess possible advantages of the former.

- To suggest design guidelines for several proposed leads. Apart from the overspill, stimulation amplitudes are also analyzed to address potential issues with safety and battery life.

Results obtained in this paper suggest that a simplified DBS model can reasonably well predict which contact or contacts are used for stimulation by medical personnel according to clinical data, at least for the analyzed lead population. Further, the described optimization algorithm obtains a significant improvement in the overspill with field steering asymmetrical stimulation compared to symmetrical stimulation provided by a state-of-the-art lead. In addition, the proposed approach makes a useful design tool for new leads, although given the variability of clinical data drawing reliable conclusions is difficult.

The rest of the paper is composed as follows. In Section II, an overview of the FEM mathematical model is given, along with different neuronal stimulation quantification schemes. Afterwards, the core optimization technique used is presented. The state-of-the-art lead is analyzed in Section III with one or two contacts used for stimulation. The field steering lead is analyzed and compared with the state-of-the-art one in Section IV. In Section V, hypothetical electrode designs are analyzed and the results obtained summarized. Conclusions and limitations are discussed in Section VI.

II. MODELS AND METHODS

In this section, the FEM model, the neuronal stimulation quantification scheme and the optimization procedure used for this study are described in detail.

A. Electric Field Model

The first step to compute optimized stimuli is to obtain the electric field distribution given the lead geometry. The electric potential is evaluated by solving the equation of steady currents in the brain tissue:

$$\nabla \cdot (\sigma \nabla u) = 0, \tag{1}$$

where u is the electric potential, σ the electric conductivity, and ∇ is the gradient operator. The electric field $\mathbf{E}$ is obtained by taking the negative gradient of u:

$$\mathbf{E} = -\nabla u. \tag{2}$$

An analytical solution to the model given by (1) does not exist in most cases, but it can be integrated numerically using, e.g., a FEM solver. The model considered in this study consists of three main components: the bulk brain tissue, the lead, and an encapsulation layer surrounding the lead.

The bulk tissue is represented as a cube with a side of 0.4 m centered at the tip of the lead that is grounded on the outer surfaces to simulate the ground in the implanted pulse generator. Although the brain tissue is heterogeneous and anisotropic in reality, these effects are beyond the scope of this paper, see [14] and [19] for details. Although the brain tissue is made of several components, e.g., white matter, gray matter, cerebrospinal fluid and blood vessels, its conductivity is approximated for this study as homogeneous with $\sigma = 0.1$ S/m [20].

In addition to the former two components, an encapsulation layer is formed around a lead implanted in the brain due to the reaction of the body to foreign objects [21]. However, the thickness and conductivity of it are still open to debate and might be patient specific. Following [14], a 0.5 mm thick layer with a conductivity of 0.18 S/m is introduced.

Several lead designs are considered in this study:

- A widely used state-of-the-art lead (Fig. 1(a)) with cylindrical contacts, a height of 1.5 mm, and a separation between contacts of 0.5 mm. Its diameter is 1.27 mm.

- A field-steering lead with elliptical contacts. To facilitate field steering, the rows are rotated 45° to each other with respect to the lead axis, as shown in Fig. 1(b),1(c), and 1(d). Its diameter is 1.27 mm as well.

- Hypothetical leads derived from the state-of-the-art one. Two design degrees of freedom are considered:
  - Row segmentation: As seen in Fig. 2, one possibility is to split each row in a number of contacts. For this study, rows with 2, 3, 4 and 6 contacts are considered.
  - Row separation: Different separation schemes are simulated to investigate the influence of other contacts' proximity on the shape of the electric field. In this study, contact row separations are in the range 0.25-1.5 mm. For comparison, depending on the lead model, the state-of-the-art leads have separations of 0.5 or 1.5 mm between contacts.

The stimulation signal is modeled as a Dirichlet boundary condition at the active contacts surface while the non-active contacts are left floating. It should be noted that model (1) is a linear partial differential equation, and thus, it is enough to compute the field distribution for a unit stimulus and then scale it accordingly, which transformation will simplify the computations.

The model has been implemented in COMSOL 4.3b (Comsol AB, Sweden). The solutions obtained by the FEM solver were then equidistantly gridded on a $70 \times 70 \times 60$ grid centered at the lead tip and expanding 16 mm in the axes perpendicular to the lead and 20 mm in the lead axis, in order to be exported for further processing.

Several field distributions were computed:

- State-of-the-art lead: Distributions with one active contact and the rest floating were evaluated at first. In addition to that, field distributions with the grounded inactive contacts were computed. This was done to enable summing up them for the multicontact approach, since the effect of one active contact on the others when they are left floating can be computed.

- Field steering lead: Distributions for the considered configurations (Diamond-4, X-5, X-8, shown in Fig. 1) were obtained for each row of contacts.

- Hypothetical leads: Similarly to the computations for the state-of-the-art leads, field distributions for one active contact with the rest floating were computed at first and, in addition, distributions with grounded inactive contacts were computed for the multicontact approach. It is useful in particular when considering two rows stimulating with different amplitudes.

B. Quantification of activated volumes

Volumes of activated tissue can be quantified by using axon models [22]. While axon models yield precise results, the procedure is computationally expensive and the topology and connectivity of the neuron network must be known to some degree. Other approaches involve functions that approximate the activated volume without taking into account the anatomy of the neurons, such as Rattay's activation function [23] or the electric field [24]. These have the advantage of requiring less computations and only stationary analysis. However, using second derivatives might result in numerical issues, in particular in the area near the lead. Furthermore, it was shown that the electric field provides more robust means of quantifying neuronal stimulation [24]. Thus, the electric field will be used in this study. The activated neurons are distinguished from the rest by applying a threshold to the electric field, with the threshold value depending on the neuron anatomy and the characteristics of the stimulation pulse itself [24].

To place the electric field pre-computed by the FEM solver at the proper position, conventional translation-rotation algebra is utilized. Assuming that the tip of the lead is at the origin, the set of operations is given by:

$$\mathbf{E}_{\text{eval}} = R_{\text{rot}} R_z \mathbf{E} + \mathbf{x}_{\text{lead}}, \qquad (3)$$

where $\mathbf{E}$ and $\mathbf{E}_{\text{eval}}$ are the original and positioned electric field vectors respectively, R_{rot} is a rotation matrix that aligns the field with the given lead vector, R_z is a rotation matrix with respect to the Z axis (used for field steering), and $\mathbf{x}_{\text{lead}}$ is the lead position.

Once the field is properly positioned and filtered with the aforementioned threshold, intersection volumes are computed under a methodology similar to [25]. Two of them are of particular interest with respect to the clinical applications: the activated volume of the target area and the activated volume outside the target area. The topology of the target area is taken from an atlas of potential regions for therapeutical stimulation and can be assumed to be convex. Whether the electric field points are inside of the convex hull of the target area or not is checked by an additional function [26].

C. Optimization scheme

In order to optimize the stimuli, the following minimization problem is defined:

$$\min_{u_i} \; J(u_i), \tag{4}$$

where u_i are the optimization variables (in this case, the electric potential or potentials of the stimuli) and $J(u_i)$ is a cost function to be defined that should ideally be a convex function.

The following cost function is proposed:

$$
\begin{aligned}
J(u_i) &= p_{\text{Spill}}(u_i) \left(\frac{100 - p_{\text{Act}}(u_i)}{100 - p_{\text{Th}}} \right) & p_{\text{Act}} \leq p_{\text{Th}}, \\
J(u_i) &= p_{\text{Spill}}(u_i) & p_{\text{Act}} > p_{\text{Th}},
\end{aligned}
\tag{5}
$$

where p_{Spill} is the fraction of the activated volume that lies outside the target, p_{Act} is the fraction of the target that is activated, and p_{Th} is the minimum activation required for the target. All of them are given in percent for illustration. For this study, p_{Th} is set at 95%. It should be noted that, if several amplitudes were to be optimized, the cost function would be multi-dimensional.

The motivation behind the cost function above is that it is continuous and convex, since both p_{Act} and p_{Spill} are monotonically non-decreasing with the amplitude of the stimulus. However, there is no clear relationship between the functions p_{Act}, p_{Spill} and the stimulus amplitudes u_i. Therefore, a numerical optimization algorithm estimating the gradient of $J(u_i)$ from the computed values of p_{Act} and p_{Spill} has to be used.

An example illustrating the dependence of cost function (5) on the stimuli amplitude is given in Fig. 3.
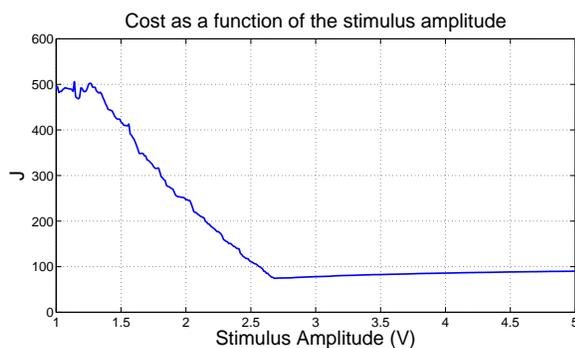

Figure 3. Example of cost function J as a function of the stimulus amplitude.

The small peaks in Fig. 3 occur because of issues with the volume computation, namely since the geometry used for both the activation volume and the target is defined in convex hulls of a discrete cloud of points. The computed volumes are thus not smooth as u changes. Although this makes the function non-convex in practice, the peaks are small enough to be skipped by increasing the step size of the optimization algorithm. A minimum step size of 0.002 V was taken.

When considering several stimulation amplitudes, extra care should be exercised then in choosing the initial guess in the optimization algorithm. It was found that the optimization gets stuck in local minima more easily than in the one-dimensional case.

III. STATE-OF-THE-ART LEAD

In this section, approaches to stimulation with the state-of-the-art lead are analyzed and compared.

A. Single Contact

To optimize stimulation with only one active contact, two approaches can be considered. First, the active contact position can be fixed and only the stimulus amplitude is optimized. Second, the active contact is left as an additional optimization variable, restricted to taking a single value in the set of possible positions $C_s = \{0, 1, 2, 3\}$, where contact 0 is the most distal and 3 is the most proximal. Due to the possibility of choosing the active contact at will and to illustrate the efficiency of the optimization method, the second approach is selected further.

Keeping the active contact free makes the optimization problem equivalent to four such with fixed contacts. In order to speed up the computations, best active contact could be chosen without optimization. By examining $J(u_i)$ given by (5), it can be easily seen that as long as there is an intersection between the activated volume and the target for at least one of the contacts, the cost function will be lower in general for the optimal contact no matter how large u_i is. So, it is enough to do a single evaluation of the cost function for a given value of u_i to choose the contact. Said value cannot be too low, since it might yield empty intersections, or too high, since it will take too much time to calculate due to the number of points involved. Thus, the evaluation is performed with low u_i and then, if the intersection is empty, u_i is set to a higher value.

Optimization was performed for 65 lead positions whose clinical data stated a single contact stimulation with an activation threshold of 175 and 200 V/m. Comparing the optimized results to the clinical settings is of great interest, so the fraction of configurations estimated successfully by the optimization algorithm with respect to the clinical settings was computed as well.
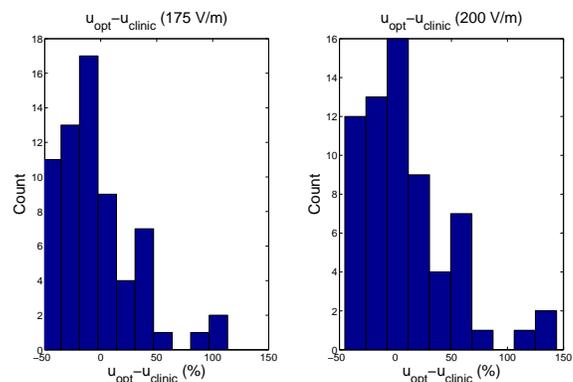

Figure 4. Discrepancy in amplitude for the optimized and clinical setting with the threshold values of 175 and 200 V/m.

As seen from Tab. I, the mathematical model predicts the clinically used contact for the defined target in roughly a half of the cases. In addition, in almost all of the cases, the predicted optimal contact is an immediate neighbor of the one specified in the clinical data. In some cases, there is no significant difference in the values of the cost function and either contact can be utilized, according to the calculated values.

TABLE I. SINGLE CONTACT OPTIMIZATION

Threshold: 200 V/m	
Correct contact (%):	53.8
1 contact error (%):	35.4
Discrepancy in amplitude (%, mean$\pm\sigma$):	9 ± 41
Threshold: 175 V/m	
Correct contact (%):	50.7
1 contact error (%):	38.4
Discrepancy in amplitude (%, mean$\pm\sigma$):	-4 ± 35

In addition, the predicted optimized stimuli amplitude is fairly close to the clinical one. The plots in Fig. 4 suggest that in most cases a threshold between 175 and 200 V/m might be sufficient. It comes though with a high standard deviation thus revealing a high variability between patients. This is to be expected, since the position of the lead has a very significant impact on the predicted optimal stimuli amplitude.

B. Multiple Contacts

Another approach to improve target coverage would be to allow for multiple active contact configurations. To facilitate the field modeling, the linearity of (1) is exploited. In particular, the field distribution for each contact stimulating with a unit stimulus while the others are grounded is computed first and denoted as $\mathbf{E}_{0,i}$ for the i-th contact. Then the interaction between active contacts and the rest in floating configuration is calculated. It follows a linear relationship and is expressed by the coefficient α_{ki}, representing the effect the i-th contact has on the k-th contact when the k-th contact is floating. This is used to transform from an active-grounded to an active-floating configuration, when the contributions are being summed.

The electric field distributions result from a sum of four contacts, with the stimuli given by the active contacts, denoted by u_i and representing the degrees of freedom and the non-active (floating) contacts contributing with the terms characterized by the corresponding α_{ki}. For instance, for a 2-contact scheme, one gets

$$\mathbf{E}_{2cont}(\mathbf{r}) = u_1\mathbf{E}_{0,1} + u_2\mathbf{E}_{0,2} + \\ + (u_1\alpha_{31} + u_2\alpha_{32})\mathbf{E}_{0,3} + (u_1\alpha_{41} + u_2\alpha_{42})\mathbf{E}_{0,4} \quad (6)$$

It should be noted that the numbering of the contacts above was arbitrary, and it could be any combination of them.

| (a) | (b) |
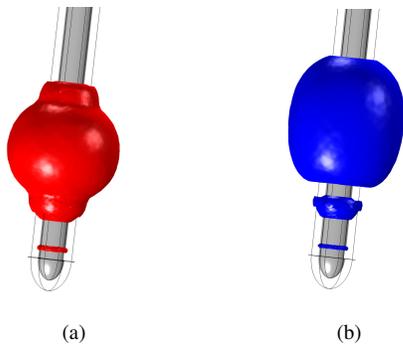
Figure 5. Isolevels for $E = 200\ V/m$ for a single active contact (a) and two active contacts (b).

As Fig. 5(b) suggests, multiple active contacts might be useful to tailor the stimulation so that it achieves a similar

activated volume with less overspill. The results are in principle dependent on the position of the target with respect to the active contact in the single contact approach. If the target is located next to the active contact, then it would be probably reasonable to consider just a single contact stimulation. However, if the target is located in between two contacts, shaping the stimulation with these two contacts might be beneficial.
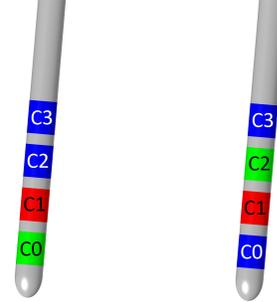

Figure 6. Example of considered multicontact configurations, with Contact 1 as the optimal (in red) and Contacts 0 (left) and 2 (right) as secondary (in green).

To speed up computations, only the configurations which involve neighboring contacts to the ones obtained in the single contact approach are considered. So, for example, if the predicted optimal contact is contact 1, only combinations involving contacts 1 and 0 and 1 and 2 are considered, see Fig. 6.
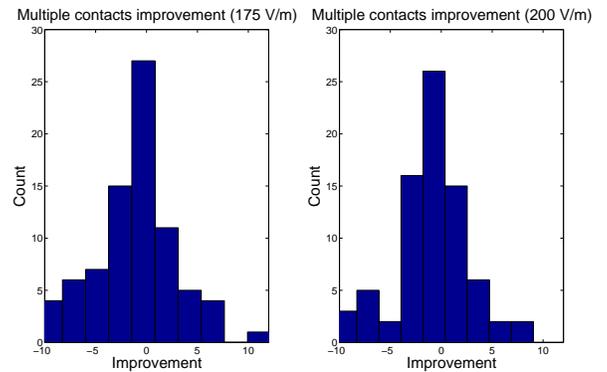

Figure 7. Improvement of overspill for 175 and 200 V/m for the multicontact approach.

TABLE II. DUAL-CONTACT OPTIMIZATION

Threshold: 200 V/m	
Improvement cases (%):	38.7
Overspill improvement (percentage points, mean$\pm\sigma$):	2.00 ± 2.28
Threshold: 175 V/m	
Improvement cases (%):	37.5
Overspill improvement (percentage points, mean$\pm\sigma$):	2.67 ± 2.83

The results are summarized in Fig. 7 and Tab. II. As expected, the improvement is situational, and appears only in a part of the cases. However, the improvement can be significant, with a decrease of up to $5-6\%$ in the absolute value of the overspill compared to the single contact approach. Note

that the state-of-the-art lead considered here features a fixed distance between contacts. The effects of uneven separation between contact rows will be analyzed later in this study.

IV. FIELD STEERING ELECTRODE

As was investigated in [25], [27], field steering yields better results regarding overspill than the state-of-the-art radial stimulation. In this study, optimization is used in order to *in silico* confirm those findings.

Three configurations llustrated in Fig. 1 were tested. For each configuration, the parameters to optimize are the rows where the active contacts are located and the orientation of the lead with respect to its axis. To speed up computations, the optimization followed a similar scheme to that applied with multiple contacts, taking as a baseline the results obtained with single contacts and the state-of-the-art lead. As shapes of the contacts are different, the rows at roughly the same height are considered, together with their neighbors.
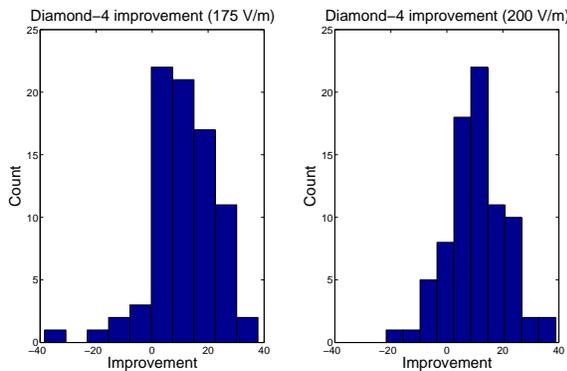
Figure 8. Improvement distribution using the Diamond 4 configuration.

TABLE III. DIAMOND 4 CONFIGURATION IMPROVEMENT.

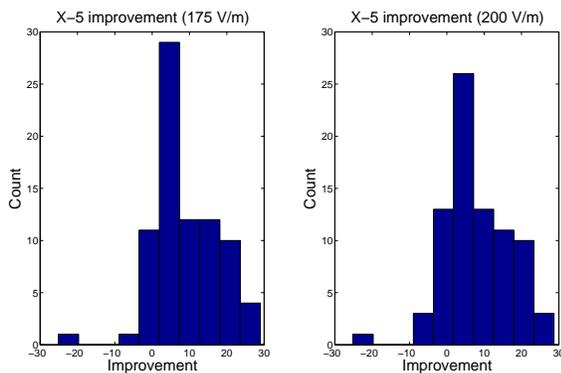| **Threshold:** 200 V/m	
Improvement cases (%):	87.5
Overspill improvement (percentage points, mean$\pm\sigma$**)**:	10.37 ± 10.52
Threshold: 175 V/m	
Improvement cases (%):	91.25
Overspill improvement (percentage points, mean$\pm\sigma$**)**:	11.48 ± 11.63

Figure 9. Improvement distribution using the X-5 configuration.

Table IV. X-5 configuration improvement

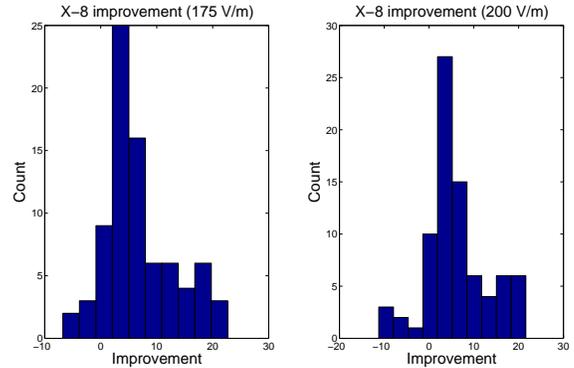| **Threshold:** 200 V/m	
Improvement cases (%):	88.75
Overspill improvement (percentage points, mean$\pm\sigma$**)**:	8.65 ± 10.67
Threshold: 175 V/m	
Improvement cases (%):	92.5
Overspill improvement (percentage points, mean$\pm\sigma$**)**:	9.76 ± 10.37

Figure 10. Improvement distribution using the X-8 configuration.

The results are summarized in Fig. 8 - Fig. 10 and Tab. III - Tab. V. In almost all cases, there is an improvement in the overspill with respect to the single contact approach. The improvement is largest in average with the Diamond-4 configuration, Fig. 8. The high standard deviation comes from the variety of geometries considered, making the improvement heavily dependent on the lead position with respect of the target. Some cases were observed where the X-5 or X-8 configurations achieved better results for a specific lead location.

V. HYPOTHETICAL LEADS

Leads that have not been implemented in hardware are analyzed in this section by computing field distributions with one or several active contacts, similarly to what has been done above for the state-of-the-art and field steering lead. This part of the study is organized in three sections:

- **Row separation comparison**, where the influence of row separation on the stimulation field is evaluated, cf. Fig. 11(a) and Fig. 11(b).

- **Row segmentation comparison**, in order to understand how many contacts per row are enough to achieve good selectivity, cf. Fig. 11(b) and Fig. 11(c).

- **Configuration comparison**, to compare active contact schemes. For each lead, three active contact configurations are considered: single contact, multiple contacts

Table V. X-8 configuration improvement

Threshold: 200 V/m	
Improvement cases (%):	90
Overspill improvement (percentage points, mean$\pm\sigma$**)**:	11.51 ± 10.63
Threshold: 175 V/m	
Improvement cases (%):	91.25
Overspill improvement (percentage points, mean$\pm\sigma$**)**:	11.56 ± 10.41

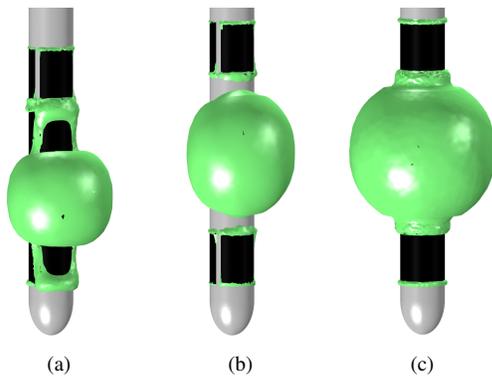(usually two) with the same amplitude and multiple contacts with different amplitudes.

Figure 11. 200 V/m isolevels for a hypothetical lead with 3 contacts per row and separation between rows of 0.25 mm (a) and 1.5 mm (b). A lead of 1 contact per row and separation of 1.5 mm is depicted for comparison (c).

Due to the amount of combinations needed, this part is limited to a population of 6 leads, with only the illustrative cases being described.

A. Row separation comparison

The first question to look into is how the separation between rows affects the predicted stimuli amplitude, together with the overspill percentage. For the state-of-the-art lead considered in the present manuscript, the separation between the rows is 0.5 mm. Separations between rows equal to 0.25 mm, 0.75 mm, 1 mm and 1.5 mm are analyzed further.

Considering only one active contact, two trends were observed, as illustrated in Fig. 12 and Fig. 13. In some cases, increasing the distance between the contacts decreases the overspill, while in some other cases the effect is the opposite one.
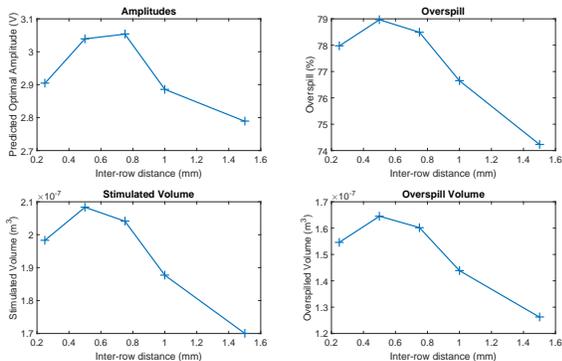

Figure 12. Predicted amplitudes, overspill percentage and activated and overspilled volumes for a single contact with 1 contact per row lead configuration.

When analyzing dual contact configurations, however, the trend is usually that the overspill is larger the more separated the contacts are, as seen in Fig. 14 and Fig. 15.

A plausible explanation for this is that the geometry of the electric field isolevels is quite different in case when the
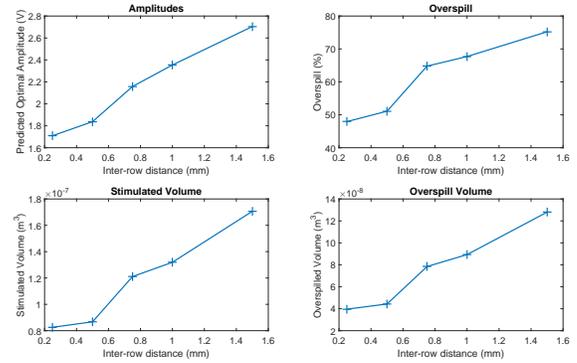

Figure 13. Predicted amplitudes, overspill percentage and activated and overspilled volumes for a single contact with 1 contact per row lead configuration.
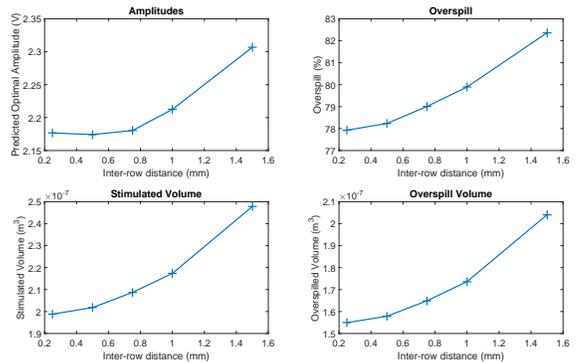

Figure 14. Predicted amplitudes, overspill percentage and activated and overspilled volumes for two active contacts in different rows with 1 contact per row lead configuration.
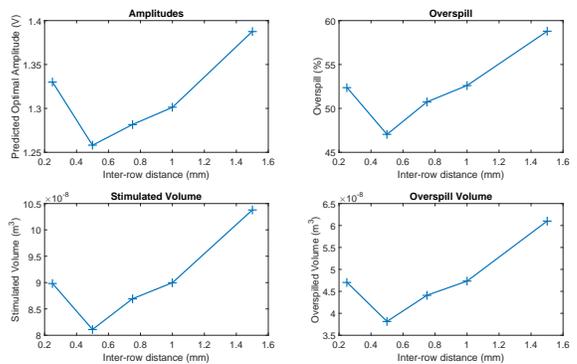

Figure 15. Predicted amplitudes, overspill percentage and activated and overspilled volumes for two active contacts in different rows with 1 contact per row lead configuration.

contacts are close to each other compared to when they are more separated. Indeed, it can be seen in Fig. 16 that the considered isolevel when contacts are close to each other is not so different from that when only one contact is active. However, when contact rows become more and more separated, the field will stretch along the lead axis. Together with the target morphology, this might explain why the overspill is larger the more separated the contacts are.
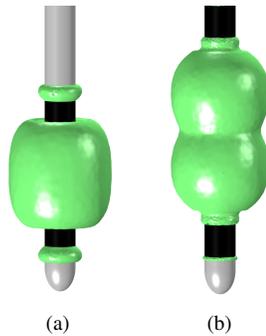

(a)   (b)

Figure 16. 200 V/m isolevels for a hypothetical lead with 1 contact per row and separation between rows of 0.25 mm (a) and 1.5 mm (b).

It can be concluded that having a large separation between contacts does not facilitate achieving a good stimulation performance although it might be beneficial in some cases when considering only one active row.

B. Row Segmentation

Another possibility to look into is segmented contact rows that also offer field steering, but for a lead shape different from that analyzed in Section IV. For this part of the study, field distributions were optimized for 1, 2, 3, 4 and 6 contacts per row, see Fig. 2. From the results obtained above for the field-steering electrode, it is expected that the overspill will decrease to some extent for the segmented state-of-the-art lead, as the segmentation increases.

In the population considered, an overspill reduction is achieved in most cases when the contacts are segmented, as illustrated in Fig. 17. However, in some other cases, probably due to the location of the lead, segmentation can actually lower the predicted performance, as shown in Fig. 18. However, these cases are less frequent.

It can be seen as well that the optimal stimulation amplitude increases as the rows become more segmented. In the population considered, the lower values of overspill with a moderate amplitude are usually obtained at three or four contacts per row at most. Going beyond that implies a large stimulation amplitude that could be potentially harmful to the patient and will consume more energy in a battery-driven device, while the benefits could be minimal or non-existent. In addition, more complex hardware could be needed in order to achieve it, thus making the product more costly and difficult to handle in the clinic.

It is worth mentioning that even in cases when segmentation does not improve the overspill, multiple contacts could be active in the same row yielding something similar to a symmetric stimulation in the state-of-the-art lead. Indeed, as can be seen in Fig. 19, there is no significant difference
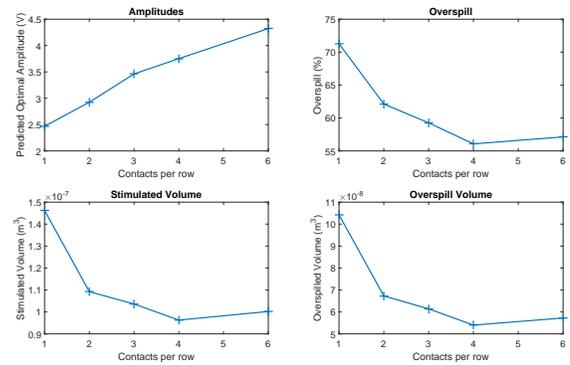

Figure 17. Predicted amplitudes, overspill percentage and activated and overspilled volumes for one active contact and different number of contacts per row. Distance between rows of 0.5 mm.
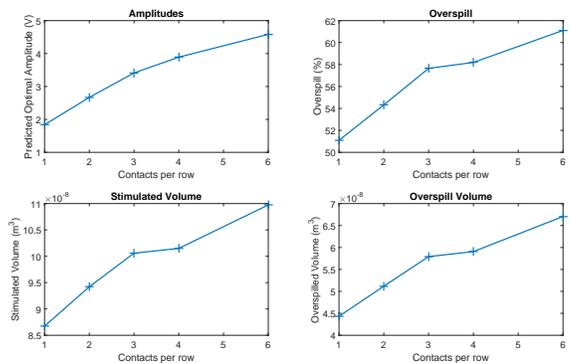

Figure 18. Predicted amplitudes, overspill percentage and activated and overspilled volumes for one active contact and different number of contacts per row. Distance between rows of 0.5 mm.

between them. Thus, even in cases when field steering does not produce an improvement, a good stimulation result can still be achieved with these hypothetical leads by making all the contacts in a given row active.
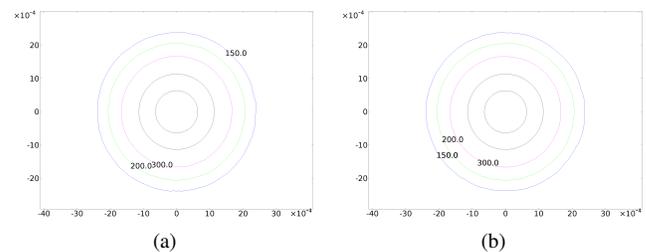

(a)   (b)

Figure 19. Contour plots taken at the middle point of a contact for a 1 contact per row lead (a) and a 6 contacts per row lead (b) for levels of electric field of 150 (blue), 200 (green) and 300 (magenta) V/m.

C. Contact configurations

Contact configurations can be analyzed, in pursuit for an improvement over the single contact ones. A more thorough analysis than in Section III is conducted here, taking into

consideration row segmentation and separation as well, since it was previously done only with the state-of-the-art lead specifications.

Dealing with active contact settings, the first issue to consider is the number of independent electrical sources present in the pulse generator. If only one is present, the same amplitude must be used for all active contacts. With several sources, different amplitudes can be assigned to the active contacts, making the setting more versatile. However, having several sources makes the hardware more complex and expensive. Further, the number of active contacts should be considered, along with their location that can be in the same row or in different rows.

For this study, configurations with both the same amplitude and different amplitudes are considered. In all cases, the active contacts neighbor each other.

1) Same amplitude: When considering active contacts with the same amplitude, two options can be analyzed: when the active contacts are in the same row or when they are in different rows. The former however is not interesting since it should yield the same stimulation as an electrode with contacts per row and one active contact. For example, if a six contacts per row lead is considered, having two active contacts in the same row means that the stimulation will be the same as with three contacts per row. Thus, only different rows are considered in this part of the study.

Some results are depicted in Fig. 20 and Fig. 21. The observed trends included the following:

- Significantly reduced amplitude in all cases, with the effect being more pronounced the more segmented the contacts are.

- When considering overspill, there is an improvement in some cases. Said improvement varies however significantly between leads: in some cases the improvement is larger with a very segmented lead and vice versa in others. As mentioned before, this is not an issue since segmented electrodes can behave as non-segmented ones, see Fig. 19.
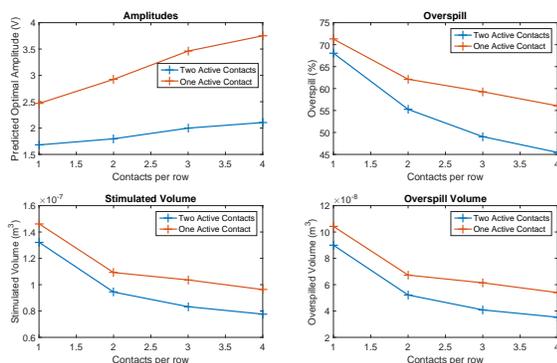

Figure 20. Predicted amplitudes, overspill percentage and activated and overspilled volumes for two active contacts (same amplitude) and different number of contacts per row. Distance between rows of 0.5 mm.

Although in some situations the overspill difference is not significant and it could be even worse when considering
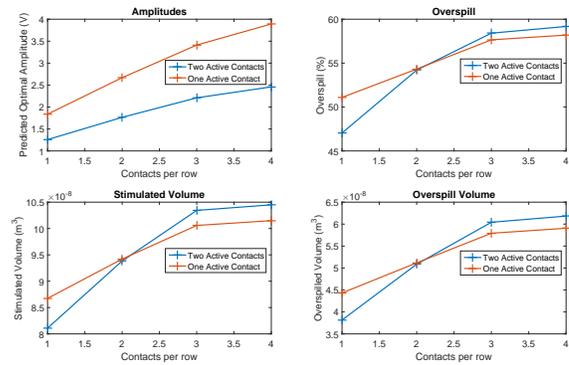

Figure 21. Predicted amplitudes, overspill percentage and activated and overspilled volumes for two active contacts (same amplitude) and different number of contacts per row. Distance between rows of 0.5 mm.

different rows, the predicted amplitude is much lower, which property translates into less power consumption and higher patient safety.

2) Different amplitude, different rows: As with the state-of-the-art lead, different stimulation amplitudes can be considered as well under the same methodology as in Section III. Different segmentation schemes will be considered as well.
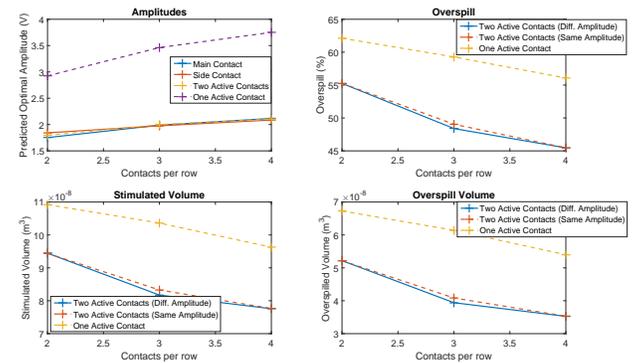

Figure 22. Predicted amplitudes, overspill percentage and activated and overspilled volumes for one and two active contacts and different number of contacts per row. Distance between rows of 0.5 mm.

From the plots in Fig. 22 and Fig. 23, the following can be concluded:

- The predicted amplitudes when different amplitudes are allowed are similar to the ones obtained with the same amplitude at all active contacts.

- Compared to the case of two contacts with the same amplitude, taking different amplitudes improves in some cases the overspill.

- In all considered cases, the amplitudes are lower than the ones obtained with only one active contact.

Thus, as expected from the results in Section III, it could be relevant in some cases to consider different amplitudes assigned to two different contacts. However, in principle, the gains might not justify the extra costs in hardware and in programming time.
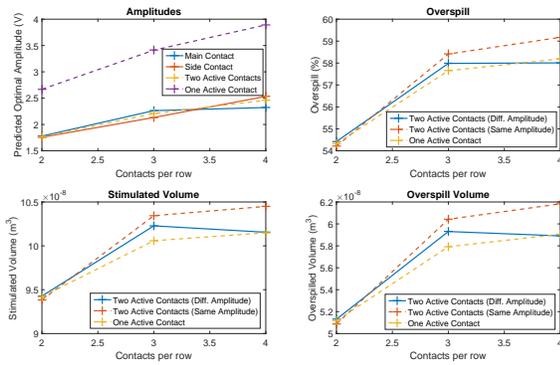
Figure 23. Predicted amplitudes, overspill percentage and activated and overspilled volumes for one and two active contacts and different number of contacts per row. Distance between rows of 0.5 mm.
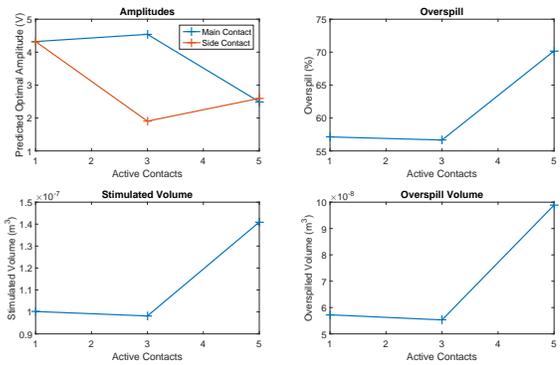

Figure 25. Predicted amplitudes, overspill percentage and activated and overspilled volumes for different active contacts. Distance between rows of 0.5 mm.

3) Different amplitude, same row: It could be interesting to see how using different stimulation amplitudes can help when the active contacts are taken in the same row. For this part, only the lead with six contacts per row is considered since it makes the most illustrative case. Configurations of three and five active contacts positioned are considered, as in Fig. 24.
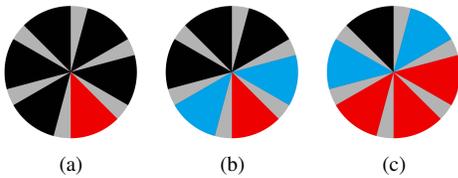

Figure 24. Configurations considered in the different amplitude, same row case. Active contacts are depicted in red and blue, with the red contacts having different amplitude than the blue contacts. Non-active contacts are depicted in black.
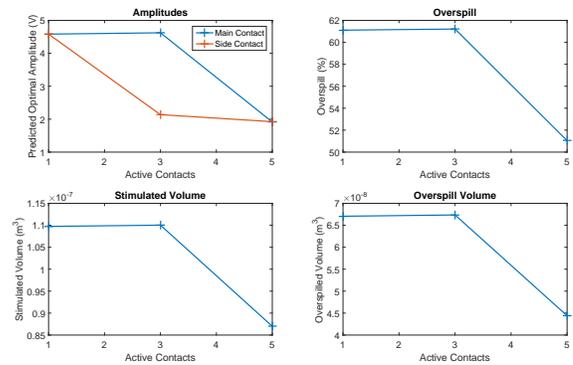

Figure 26. Predicted amplitudes, overspill percentage and activated and overspilled volumes for different active contacts. Distance between rows of 0.5 mm.

The results obtained show that there is indeed a possibility of using these configurations, as can be seen in Fig. 25 and Fig. 26. Surprisingly, with five active contacts, the predicted amplitudes are mostly the same for all contacts, which does not happen when three active contacts are considered. However, the results exhibit large variability and can make this alternative not worth the effort. Nevertheless, it could clearly improve the performance in some cases.

VI. DISCUSSION

Using optimization schemes in order to scale the stimulus amplitude of the active contact or contacts could yield an activation volume that better covers a given target while limiting, as much as possible, stimulation beyond the target. This study has compared two available leads: a state-of-the-art lead and a field steering lead. In addition, several hypothetical leads have been tested in order to gain an insight into lead design. Different contact configurations have been tested as well.

Selecting the active contact freely for a given target with the state-of-the-art lead while using the single-contact approach, a simple model predicts the clinically used contact in roughly a half of the times in the considered lead population.

Furthermore, in some cases, there is no significant difference between the amplitudes or performance of the clinical and the optimal configurations. Extending the stimulation to multiple contacts allowed for an improvement of the overspill in around 38% of the cases.

The obtained results were compared to field steering configurations. A significant improvement of the overspill with a decrease of 10 percentage points on average was found in all cases, with an average decrease of 18 percentage points for the Diamond 4 configuration.

The analysis was then extended to hypothetical leads with a significant variability in results observed. Even so, some trends have been discerned: higher vertical separation between the contacts usually leads to a higher overspill, in particular when multiple active contacts are considered. Segmentation yields good results in most of the analyzed leads, with the best performance achieved with three or four contacts per row. Even if no improvement is present, it is still possible to stimulate in a way similar to the state-of-the-art lead by making all contacts in the same row active. Care should be exercised however, since the amplitudes needed to achieve satisfactory coverage are higher than in the non-segmented leads, an effect that becomes more profound the more segmented the leads are. When stimulating

with several contacts, the amplitude is significantly lower but a higher overspill could occur. Nevertheless, variability among patients makes it difficult to achieve general conclusions in many cases.

The results obtained in this study apply under some limitations. First, the brain tissue was assumed to be homogeneous, when this is not the case and significant (patient specific) differences may arise [14]. Furthermore, the encapsulation layer surrounding the lead has uncertain physical properties, such as the conductivity and the thickness, both of which might be time varying [28]. In addition, considering the electric field as a predictor of whether a neuron is stimulated or not is an approximation. A more thorough analysis would need a complete neuron population model. Finally, the results obtained assume a certain target structure, which may be patient specific as well. Results should be verified against therapeutic outcomes, but the latter were not available for this study.

Despite the mentioned limitations, this study highlights the use of optimization schemes and geometric arguments to choose optimal DBS stimuli and facilitate the comparison between different lead designs and contract configurations. These optimization schemes could be used as a benchmark for other optimization algorithms such as in [29] and the intersection algorithms can be used in order to assess a set of stimulation settings as in [25].

REFERENCES

[1] R. Cubo, M. Åström, and A. Medvedev, "Model-based Optimization of Lead Configurations in Deep Brain Stimulation," 1st IARIA International Conference on Smart Portable, Wearable, Implantable and Disability-oriented Devices and Systems (SPWID), Brussels, Belgium, 2015, pp. 14-19.

[2] J. A. Obeso, C. W. Olanow, M. C. Rodriguez-Oroz, P. Crack, and R. Kumar, "Deep-Brain Stimulation of the Subthalamic Nucleus or the Pars Interna of the Globus Pallidus in Parkinson's Disease," N. Engl. J. Med., vol. 345, no. 13, 2001, pp. 956-963.

[3] N. Suthana et al., "Memory enhancement and deep-brain stimulation of the entorhinal area," N. Engl. J. Med., vol. 366, 2012, pp. 502-510.

[4] C. Hamani, S. S. Stone, A. Garten, A. M. Lozano, and G. Winocur, "Memory rescue and enhanced neurogenesis following electrical stimulation of the anterior thalamus in rats treated with corticosterone," Exp. Neurol., vol. 232, no. 1, 2011, pp. 100-104.

[5] R. Gross and A. M. Lozano, "Advances in neurostimulation for movement disorders," Neurol Res., vol. 22, 2000, pp. 247-258.

[6] J. Kuhn et al., "Deep Brain Stimulation in Schizophrenia," Fortschritte der Neurol. Psychiatr., vol. 79, 2011, pp. 632-641.

[7] V. Vandewallea, C. van der Lindena, H. J. Groenewegena, and J. Caemaert, "Stereotactic treatment of Gilles de la Tourette syndrome by high frequency stimulation of thalamus," Lancet, vol. 353, no. 9154, 1999, p. 724.

[8] A. Williams et al., "Deep brain stimulation plus best medical therapy versus best medical therapy alone for advanced Parkinson's disease (PD SURG trial): a randomised, open-label trial," Lancet Neurol., vol. 9, no. 6, pp. 581-591, 2010.

[9] J. Dams et al., "Cost-effectiveness of deep brain stimulation in patients with Parkinson's disease," Mov. Disord., vol. 28, no. 6, pp. 763-771, 2013.

[10] C. D. Marsden, "Problems with long-term levodopa therapy for Parkinson's disease," Clin. Neuropharmacol., vol. 17, Suppl 2, 1994, pp. S32-44.

[11] G. Deuschl et al., "Stimulation of the subthalamic nucleus at an earlier disease stage of Parkinson's disease: concept and standards of the EARLYSTIM-study," Parkinsonism Relat. Disord., vol. 19, no. 1, Jan. 2013, pp. 56-61.

[12] J. L. Alberts et al., "Bilateral subthalamic stimulation impairs cognitive-motor performance in Parkinson's disease patients," Brain, vol. 131, no. Pt 12, Dec. 2008, pp. 3348-3360.

[13] J. Gardner, "A history of deep brain stimulation: Technological innovation and the role of clinical assessment tools," Soc. Stud. Sci., vol. 43, no. 5, pp. 707-728, 2013.

[14] A. Chaturvedi, C. R. Butson, S. Lempka, S. E. Cooper, and C. C. McIntyre, "Patient-specific models of deep brain stimulation: influence of field model complexity on neural activation predictions," Brain Stimul., vol. 3, no. 2, 2010, pp. 65-67.

[15] H. C. Martens et al., "Spatial steering of deep brain stimulation volumes using a novel lead design," Clin. Neurophysiol., vol. 122, no. 3, Mar. 2011, pp. 558-566.

[16] J. Buhlmann, L. Hofmann, P. a Tass, and C. Hauptmann, Modeling of a segmented electrode for desynchronizing deep brain stimulation., Front. Neuroeng., vol. 4, no. December, p. 15, Jan. 2011.

[17] C. R. Butson, C. C. McIntyre, "Role of electrode design on the volume of tissue activated during deep brain stimulation," J. Neural Eng., vol. 3, 2006, pp. 1-8.

[18] B. Howell, W. M. Grill, "Model-Based Optimization of Electrode Designs for Deep Brain Stimulation," 6th Annual International IEEE EMBS Conference on Neural Engineering San Diego, California, 2013, pp. 154-157.

[19] M. Åström, J. Lemaire, and K. Wårdell, "Influence of heterogeneous and anisotropic tissue conductivity on electric field distribution in deep brain stimulation," Med. Biol. Eng. Comput., vol. 50, no. 1, 2012, pp. 23-32.

[20] D. Andreuccetti, R. Fossi, and C. Petrucci, "Dielectric properties of body tissue," 2005. Available: http://niremf.ifac.cnr.it/tissprop/ [accessed: 2016.06.05].

[21] W. M. Grill, J. T. Mortimer, "Electrical properties of implant encapsulation tissue," Ann. Biomed. Eng., vol. 22, no. 1, 1994, pp. 23-33.

[22] D. R. McNeal, "Analysis of a model for excitation of myelinated nerve," IEEE Trans. Biomed. Eng., vol. 23, no. 4, Jul. 1976, pp. 329-337.

[23] F. Rattay, "Analysis of models for external stimulation of axons," IEEE Trans. Biomed. Eng., vol. 33, 1986, pp. 974-977.

[24] M. Åström, E. Diczfalusy, H. C. Martens, and K. Wårdell, "Relationship between Neural Activation and Electric Field Distribution during Deep Brain Stimulation," IEEE Trans. Biomed. Eng., vol. 62, no. 2, 2015, pp. 664-672.

[25] R. Cubo, M. Åström, and A. Medvedev, "Target coverage and selectivity in field steering brain stimulation," 36th Annual International Conference of the IEEE EMBS, Chicago, IL, 2014, pp. 522-525.

[26] J. D'Errico. Inhull function. MATLAB File Exchange. URL: http://mathworks.com/matlabcentral/fileexchange/10226-inhull [accessed: 2016.06.05].

[27] R. Cubo, M. Åström, and A. Medvedev, Stimulation field coverage and target structure selectivity in field steering brain stimulation, Mov. Disord., vol. 29, no. S1, pp. S198-S199, 2014.

[28] S. F. Lempka, M. Johnson, S. Miocinovic, J. L. Vitek, and C. C. McIntyre, "Current-controlled deep brain stimulation reduces in vivo voltage fluctuations observed during voltage-controlled stimulation," Clin. Neurophysiol., vol. 121, no. 12, 2010, pp. 2128-2133.

[29] R. Cubo, M. Åström, and A. Medvedev, "Electric Field Modeling and Spatial Control in Deep Brain Stimulation," 54th IEEE Conference on Decision and Control, Osaka, Japan, 2015.